ACS APPLIED MATERIALS & INTERFACES

Research Article

www.acsami.org

High-Performance Organic Small-Molecule Panchromatic Photodetectors

Zisheng Su,*[,†] Fuhua Hou,[†,‡] Xing Wang,[†] Yuan Gao,[†,‡] Fangming Jin,[†,‡] Guang Zhang,*[,†] Yantao Li,[†] Ligong Zhang,[†] Bei Chu,*[,†] and Wenlian Li[†]

[†]State Key Laboratory of Luminescence and Applications, Changchun Institute of Optics, Fine Mechanics and Physics, Chinese Academy of Sciences, Changchun 130033, P. R. China

[‡]University of Chinese Academy of Sciences, Beijing, 100039, P. R. China

Supporting Information

ABSTRACT: High-performance panchromatic organic photodetectors (OPDs) containing small molecules lead phthalocyanine (PbPc) and C_{70} fullerene as donor and acceptor, respectively, were demonstrated. The OPDs had either a PbPc/C_{70} planar heterojunction (PHJ) or a PbPc/PbPc:C_{70}/C_{70} hybrid planar-mixed molecular heterojunction (PM-HJ) structure. Both the PHJ and the PM-HJ devices showed a broad-band response that covered wavelengths from 300 to 1100 nm. An external quantum efficiency (EQE) higher than 10% and detectivity on the order of 10^{12} Jones were obtained in the wavelength region from 400 to 900 nm for the PHJ device. The EQE in the near-infrared region was enhanced by using the PM-HJ device structure, and a maximum EQE of 30.2% at 890 nm was observed for the optimized device with a 5% PbPc-doped C_{70} layer. Such an EQE is the highest at this wavelength of reported OPDs. The detectivity of the PM-HJ devices was also higher than that of the PHJ one, which is attributed to the increased efficiency of exciton dissociation in bulk heterojunction structure, increased absorption efficiency caused by formation of triclinic PbPc in the PbPc:C_{70} mixed film when it was deposited on a pristine PbPc layer, and high hole mobility of the PbPc-doped C_{70} layer.

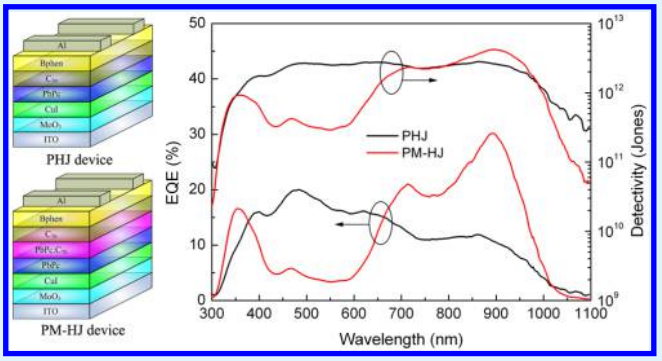

KEYWORDS: *organic photodetector, panchromatic photoresponse, small molecule, planar heterojunction, bulk heterojunction*

1. INTRODUCTION

Organic photodetectors (OPDs) have been the subject of extensive research because of their large-area detection, wide selection of suitable materials, and compatibility with flexible substrates.[1,2] Numerous OPDs for ultraviolet (UV)−visible (vis) to near-infrared (NIR) wavelengths have been demonstrated.[3−9] Recently, panchromatic OPDs with sensitivity from UV−vis to NIR wavelengths have attracted considerable attention because of their potential applications in industry and science, such as remote control, image sensing, communication, environmental monitoring, day- and nighttime surveillance, chemical/biological sensing, and spectroscopic and medical instruments.[10−18] Gong et al.[10] fabricated panchromatic OPDs containing a small-band-gap polymer poly(5,7-bis(4-decanyl-2-thienyl)-thieno(3,4-b)diathiazole-thiophene-2,5) blended with [6,6]-phenyl-C61-butyric acid methylester (PCBM) that showed a broad spectral response from 300 to 1450 nm and detectivity (D^*) of greater than 10^{12} Jones. Hu and co-workers developed high-performance panchromatic OPDs based on a donor (D)−acceptor (A) copolymer.[11] Hendriks et al.[12] demonstrated a series of small-band-gap polymers with high photoresponse at NIR wavelength. Although high-performance panchromatic OPDs based on polymers have been demonstrated, it is difficult to achieve even higher efficiency in polymer systems because of the lack of precise control of their polydispersity index, regioregularity, and molecular weight. These parameters have to be considered in thin-film processing and are strongly correlated with the detection performance of the OPD. Materials with low molecular weight are an alternative to polymers for use in panchromatic OPDs. Zimmerman et al.[13] developed a panchromatic OPD based on a porphyrin-tape/C_{60} heterojunction that exhibited an external quantum efficiency (EQE) of 6.5% at 1350 nm. The EQE of this OPD was enhanced to 13.5% at 1385 nm by adding 4,4′-bipyridyl to the porphyrin-tape/PCBM mixture.[14] Beverina and colleagues demonstrated a panchromatic OPD based on a squaraine compound with an EQE of about 5% at 700 nm.[15] Li et al.[16] fabricated a panchromatic OPD based on a porphyrin derivative:PCBM blend with an EQE of about 23% at 800 nm at −2 V and D^* on

Received: October 27, 2014
Accepted: January 15, 2015
Published: January 15, 2015

DOI: 10.1021/am5074479
ACS Appl. Mater. Interfaces 2015, 7, 2529−2534

the order of 10^{12} Jones. A panchromatic OPD based on a D−A−D small molecule:PCBM blend with an EQE of about 10% at 800 nm at −2 V and D^* on the order of 10^{11} Jones has also been reported.[17] Menke et al.[18] constructed a panchromatic OPD by arranging three bulk heterojunctions (BHJs) in tandem; this device achieved an EQE of about 10% at 900 nm at zero bias and D^* on the order of 10^{12} Jones. Although these small-molecule panchromatic OPDs have been reported, their EQEs and D^* are still too low for practical application, especially in the NIR region. Therefore, it is desirable to further improve the performance of small-molecule OPDs.

Lead phthalocyanine (PbPc) is a shuttlecock-shaped molecule with a high absorption coefficient in the NIR region.[19−22] We previously demonstrated highly efficient NIR OPDs based on a simple PbPc/C_{60} planar heterojunction (PHJ).[23,24] The EQE of these OPDs is low at vis wavelengths because both PbPc and C_{60} absorb poorly in this region. There are two typical device structures for photodiodes, PHJ and BHJ. Compared with a PHJ device, a BHJ device shows a higher photogenerated current, which results from the increased probability of exciton dissociation caused by the decreased D−A distance. Device performance can be further improved by using a hybrid planar-mixed molecular heterojunction (PM-HJ) structure that consists of a mixed layer of D and A molecules sandwiched between homogeneous layers of the D and A materials because this structure improves the efficiency of charge carrier collection.[25] C_{70} fullerene absorbs long wavelengths more strongly than C_{60} because of a relaxation of the symmetry-forbidden transitions in C_{70}.[26] This makes C_{70} more suitable for use in panchromatic OPDs than C_{60}. In this paper, PbPc and C_{70} are adopted as the D and A, respectively, to construct panchromatic OPDs. Devices with PHJ and PM-HJ structures are fabricated, and the effects of device structure on performance are evaluated. Both structures of OPD exhibit a broad-band response from 300 to 1100 nm with high EQE and D^*.

2. EXPERIMENTAL DETAILS

Devices were fabricated on patterned indium tin oxide (ITO) coated glass substrates with a sheet resistance of 15 Ω/sq. The substrates were routinely cleaned followed by UV-ozone treatment for 10 min. The optimized PHJ device has a structure of ITO/MoO_3 (2 nm)/CuI (2 nm)/PbPc (60 nm)/C_{70} (60 nm)/4,7-diphenyl-1,10-phenanthroline (Bphen, 10 nm)/Al (100 nm), while the optimized PM-HJ device has a structure of ITO/MoO_3 (2 nm)/CuI (2 nm)/PbPc (20 nm)/PbPc:C_{70} (80 nm)/C_{70} (20 nm)/Bphen (10 nm)/Al (100 nm). The structures of the devices, PbPc, and C_{70} are shown in Figure 1. The weight ratio of PbPc:C_{70} in the PM-HJ devices was varied to determine the optimum ratio. Layers were sequentially deposited onto the substrates in sequence by thermal evaporation in a vacuum chamber at a pressure of 5×10^{-4} Pa without breaking vacuum. Deposition rate and layer thickness were monitored in situ using oscillating quartz monitors. Evaporation rates were kept at 0.2 Å/s for MoO_3 and CuI, 1 Å/s for the organic layers, and 5 Å/s for the Al cathode. EQE spectra were obtained with a lock-in amplifier (Stanford SR830) under monochromatic illumination at a chopping frequency of 130 Hz using a chopper (Stanford SR540). The dark currents of the devices were measured with a source meter (Keithley 2400). Absorption spectra were recorded on a spectrophotometer (Lambda 900). Grazing incidence X-ray diffraction (GIXRD) patterns were measured with a diffractometer (Rigaku D/Max-2500) using Cu Kα radiation (λ = 1.54056 Å). Optical properties of the films were measured by spectroscopic ellipsometry (AST SE200BM). All measurements were performed under ambient conditions.

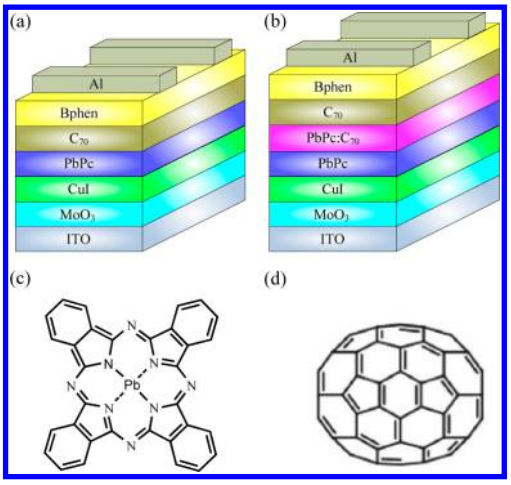

Figure 1. Structures of (a) PHJ OPD, (b) PM-HJ OPD, (c) PbPc, and (d) C_{70}.

3. RESULTS AND DISCUSSION

Figure 2 shows the EQE spectrum of the PHJ device at zero bias. This device exhibits a broad-band response that covers the wavelength range from 300 to 1100 nm. The EQE of this device in the wavelength region from 400 to 900 nm exceeds 10% with a maximum of 20.0% at 484 nm. The C_{70} film has a strong absorption band in the vis region with a peak at about 530 nm, as shown in Figure 3. The PbPc film has a strong absorption band in the NIR region with two peaks at about 730 and 900 nm that are related to the amorphous or monoclinic phases and triclinic phase, respectively. Thus, the response of the PHJ device can be ascribed to the dissociation of the excitons of both PbPc and C_{70}.

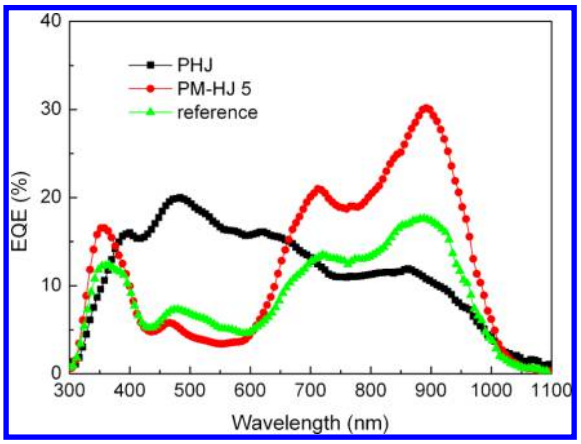

Figure 2. EQE spectra of the PHJ device ITO/MoO_3 (2 nm)/CuI (2 nm)/PbPc (60 nm)/C_{70} (60 nm)/Bphen (10 nm)/Al (100 nm), PM-HJ 5 device ITO/MoO_3 (2 nm)/CuI (2 nm)/PbPc (20 nm)/PbPc:C_{70} (80 nm, 5%:95%)/C_{70} (20 nm)/Bphen (10 nm)/Al (100 nm), and reference device ITO/MoO_3 (2 nm)/CuI (2 nm)/PbPc (20 nm)/C_{70} (100 nm)/Bphen (10 nm)/Al (100 nm).

The performance of the PM-HJ devices is closely related to the weight ratio of D:A in the mixed layers, so it is important to clarify this relationship. PM-HJ devices containing different doping concentrations of PbPc in C_{70} (0, 5%, 10%, 20%, 25%, 50%, and 75%, hereafter denoted as reference, PM-HJ 5, PM-HJ 10, PM-HJ 20, PM-HJ 25, PM-HJ 50, and PM-HJ 75 devices, respectively) in the mixed layer were fabricated.

DOI: 10.1021/am5074479
ACS Appl. Mater. Interfaces 2015, 7, 2529−2534

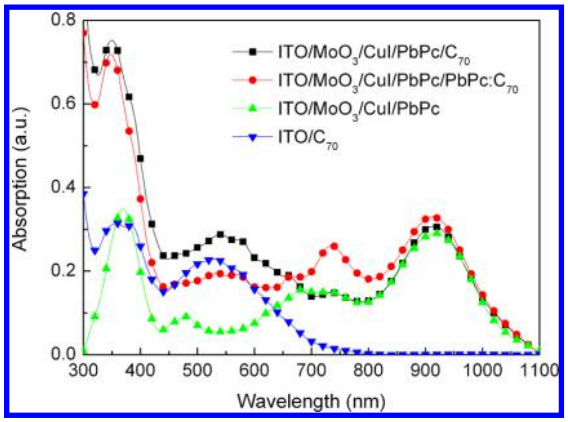

Figure 3. Absorption spectra of PbPc (20 nm)/C_{70} (80 nm), PbPc (20 nm)/PbPc:C_{70} (80 nm, 5%:95%), and PbPc (20 nm) films on an ITO/MoO_3 (2 nm)/CuI (2 nm) substrate and C_{70} (80 nm) film on an ITO substrate.

Compared with the PHJ device, the reference device has PbPc and C_{70} layers of different thickness but the same total thickness. The reference device shows a smaller response in the vis region but larger response in the NIR region compared with the PHJ device, and the maximum EQE of the reference device is 17.6% at 890 nm, as shown in Figure 2. The internal optical electric field distribution of a device can be calculated from the complex indices of refraction and layer thickness of the materials determined by spectroscopic ellipsometry.[27] Figures S1 and S2, Supporting Information, compare the calculated internal optical electric field distributions of the PHJ and reference devices. The squared optical electric field strength at the PbPc/C_{70} interface of the reference device is significantly higher than that of the PHJ device for a wavelength of 900 nm. This results in the larger response of the reference device in the NIR region. Although the reference device also exhibits a higher squared optical electric field strength at the PbPc/C_{70} interface for a wavelength of 450 nm, the thick C_{70} layer may lead to a higher recombination probability of charge carriers in the bulk of C_{70} layer and hence the smaller response in the vis region. Figure S3, Supporting Information, presents the EQE spectra of the PM-HJ devices at zero bias. Similar to the PHJ and reference devices, the PM-HJ devices also exhibit a broad-band response as expected. Moreover, the response of the PM-HJ devices decreases with increasing doping concentration of PbPc. The PM-HJ 5 device has the highest response of those examined, which indicates that loading C_{70} with just 5% PbPc can provide efficient ways for exciton dissociation and charge carrier transport in the PbPc:C_{70} mixed layer. A similar phenomenon has been found in small-molecule organic solar cells.[28−37] Compared with the reference device, the response of the PM-HJ 5 device is smaller in the vis region and larger in the NIR region. The maximum EQE of the PM-HJ 5 device is 30.2% at 890 nm, which is about 3 times larger than that of the PHJ device, 1.7 times that of the reference device, and higher than those of other OPDs at the same wavelength.[10−18]

To determine the origin of the dependence of the EQE spectrum on device structure, the absorption spectra of various films were measured, as shown in Figure 3. The PbPc (20 nm)/PbPc:C_{70} (5%:95%, 80 nm) film showed considerably stronger absorption at 730 nm and slightly stronger absorption at 900 nm compared with that of the PbPc (20 nm)/C_{70} (80 nm) film. This indicates that both amorphous or monoclinic and triclinic phases of PbPc are formatted in the PbPc:C_{70} film when it was deposited on ITO/MoO_3/CuI/PbPc. The formation of triclinic PbPc is important to increase the response of the device in the NIR region. We further assume that the formation of the triclinic phase results from the molecular interaction between the PbPc molecules in the underling pristine PbPc layer and PbPc:C_{70} mixed layer. This interaction was confirmed by considering the EQE spectrum of a device with the structure of ITO/MoO_3 (2 nm)/CuI (2 nm)/PbPc:C_{70} (100 nm, 5%:95%)/C_{70} (20 nm)/Bphen (10 nm)/Al (100 nm). This device had no response at about 900 nm because it did not contain a pristine PbPc layer between the CuI and the PbPc:C_{70} mixed layers, as shown in Figure S4, Supporting Information. The EQE spectrum of the PM-HJ 5 device is more strongly enhanced at 900 nm than that of the reference device, which is opposite behavior to the absorption spectra of these devcies. This can be well understood by the fact that the triclinic phases predominantly functioned as carrier generation sites, while the amorphous or monoclinic phases acted as hole transporting channels.[38] Figure S5, Supporting Information, shows the absorption spectra of the ITO/MoO_3 (2 nm)/CuI (2 nm)/PbPc (20 nm)/PbPc:C_{70} (80 nm) films containing different doping concentrations of PbPc in C_{70}. The absorption in the vis region decreases with increasing doping concentration of PbPc, which would result in the decrease of the EQE in this region, as shown in Figures 2 and S3, Supporting Information. On the other hand, the absorption in the NIR region increases with doping concentration of PbPc, which is contrary to the trend found in the EQE spectra of the PM-HJ devices. This indicates that there remain other factors that limit the EQE spectra of the PM-HJ devices beyond absorption.

Figure 4 shows the dark currents of the PHJ and PM-HJ 5 devices. Both devices exhibit a rectification ratio on the order of

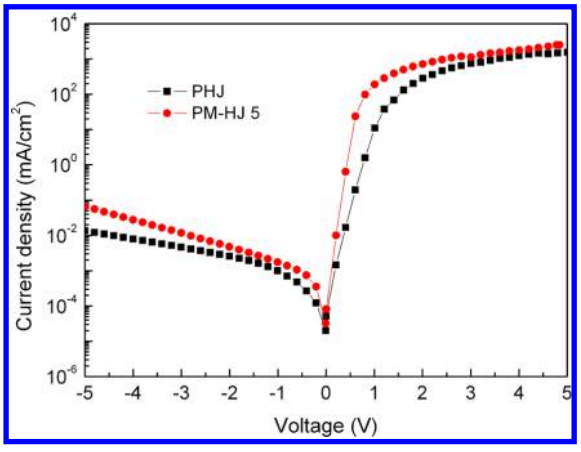

Figure 4. Dark currents of the PHJ device ITO/MoO_3 (2 nm)/CuI (2 nm)/PbPc (60 nm)/C_{70} (60 nm)/Bphen (10 nm)/Al (100 nm) and PM-HJ 5 device ITO/MoO_3 (2 nm)/CuI (2 nm)/PbPc (20 nm)/PbPc:C_{70} (80 nm, 5%:95%)/C_{70} (20 nm)/Bphen (10 nm)/Al (100 nm).

10^4 at ±5 V. Moreover, the PM-HJ 5 device has a higher current density than the PHJ device in both the positive and the negative voltage regions, indicating that the PM-HJ 5 device has higher conductivity than the PHJ one. This can be further verified by considering the current density−voltage (J−V) characteristics of the related hole- and electron-only devices. Figure 5 compares the currents of the hole- and electron-only devices with structures of ITO/organic layers/*N*,*N*′-diphenyl-*N*,*N*′-bis(1-naphthyl)-(1,1′-benzidine)-4,4′-diamine (NPB, 20

DOI: 10.1021/am5074479
ACS Appl. Mater. Interfaces 2015, 7, 2529−2534

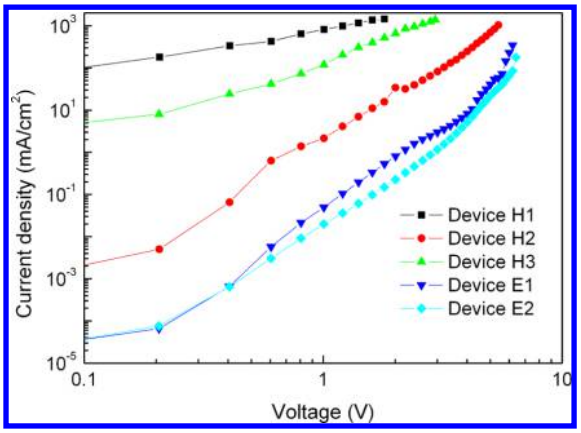

Figure 5. *J*–*V* curves of hole- and electron-only devices.

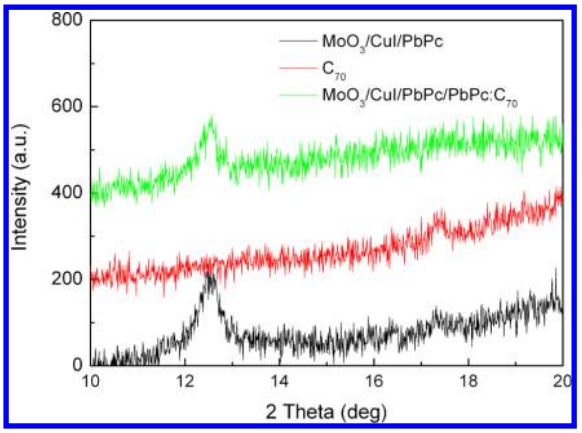

Figure 6. GIXRD patterns of MoO_3 (2 nm)/CuI (2 nm)/PbPc (20 nm), C_{70} (60 nm), and MoO_3 (2 nm)/CuI (2 nm)/PbPc (20 nm)/PbPc:C_{70} (80 nm, 5%:95%) films on ITO substrates.

nm)/Ag (100 nm) and ITO/Bphen (10 nm)/organic layers/Bphen (20 nm)/Al (100 nm), respectively, where the organic layers were MoO_3 (2 nm)/CuI (2 nm)/PbPc (100 nm) (Device H1), MoO_3 (2 nm)/CuI (2 nm)/PbPc (20 nm)/C_{70} (80 nm) (Device H2), or MoO_3 (2 nm)/CuI (2 nm)/PbPc (20 nm)/PbPc:C_{70} (80 nm, 5%:95%) (Device H3) for hole-only devices and MoO_3 (2 nm)/CuI (2 nm)/PbPc (20 nm)/C_{70} (80 nm) (Device E1) or MoO_3 (2 nm)/CuI (2 nm)/PbPc (20 nm)/PbPc:C_{70} (80 nm, 5%:95%) (Device E2) for electron-only devices. The NPB layer next to the Ag electrode in the hole-only devices restricts the injection of electrons, while the Bphen layer next to the ITO electrode in the electron-only devices restricts the injection of holes. The current density of Device H1 is about 1 order of magnitude higher than that of Device H3 at low voltage, and this difference decreases to only several times at high voltage; for example, it is about 2.8 times at 1.8 V. Although we have not obtained the accurate hole mobility of the mixed films, this result means that the PbPc-doped C_{70} film has a high hole mobility even when the concentration of PbPc is only 5%. Such a behavior is crucial to transport photogenerated holes outside the mixed layer. The current densities of Device H1 and H3 are more than 1 order of magnitude higher than that of Device H2. In contrast, Devices E1 and E2 have almost the similar current densities, suggesting that the PbPc-doped C_{70} film still retains a high electron mobility. These findings indicate that the increased dark current of the PM-HJ 5 device compared with that of the PHJ device can be attributed to doping with PbPc markedly increasing the hole mobility of the C_{70} film. The hole mobility of the C_{70} film may further increase with increasing doping concentration of PbPc and an opposite trend for the electron mobility.[28,29] The decreased electron mobility would induce serious bimolucular recombination because electrons cannot escape the blend films easily without meeting with their counterparts.[29] This may result in the decrease of the EQE of the PM-HJ devices with higher doping concentration of PbPc.

Generally, mixing D and A in the organic active layer in a BHJ device decreases the D–A distance, which increases the probability of exciotn dissociation of both D and A. This will increase the response from both D and A even when a small amount of D is present.[38] However, the response of our PM-HJ device in the vis region is decreased compared with the reference device. This means that the dissociation efficiency of C_{70} excitons is reduced, which is contrary to our expectation. Figure 6 shows the GIXRD patterns of MoO_3 (2 nm)/CuI (2 nm)/PbPc (20 nm), C_{70} (60 nm), and MoO_3 (2 nm)/CuI (2 nm)/PbPc (20 nm)/PbPc:C_{70} (80 nm, 5%:95%) films on ITO substrates. The C_{70} film exhibits a weak diffraction peak at about 17.3° that can be assigned to crystals of C_{70} in the neat film.[32] However, this diffraction peak is not observed for the PbPc:C_{70} film, indicating that the formation of C_{70} crystals is disrupted by addition of PbPc. This decrease of crystallinity may decrease the exciton diffusion length and electron mobility of the C_{70} film.[40] This effect may become more serious with higher doping concentration of PbPc. As a result, the responses of both C_{70} and PbPc in the PM-HJ devices decrease with increasing doping concentration of PbPc.

The internal optical electric field distribution inside a device is an important factor that determines the profile of its EQE spectrum. Figure S6, Supporting Information, compares the amplitude ratio and phase difference of C_{70} and PbPc:C_{70} (5%:95%) films with a thickness of 80 nm on ITO/MoO_3 (2 nm)/CuI (2 nm)/PbPc (20 nm) substrates measured with a spectroscopic ellipsometry. Both the amplitude ratio and the phase difference of these two films are similar at about 890 nm. This suggests that doping a C_{70} film with 5% PbPc does not alter its optical parameters at 890 nm, which means the internal optical electric field distribution does not contribute to the increased response of the PM-HJ 5 device in the NIR region compared with that of the reference device.

D^* is another important parameter for a photodetector, which can be calculated using the equation

$$D^* = R \cdot \sqrt{A} / S_N \quad (1)$$

where R is responsivity, A is area, and S_N is current spectral noise density. S_N^2 is the sum of all noise powers (e.g., thermal, shot, and excess noise). Under zero bias, thermal noise dominates other types of noise. In this situation, D^* can be calculated as follows[41]

$$D^* = R \cdot \sqrt{A \cdot R_D / (4 k_B T)} \quad (2)$$

where R_D is the zero-bias differential resistance of the device, k_B is the Boltzmann constant, and T is temperature. D^* of the PHJ and PM-HJ 5 devices are shown in Figure 7. D^* of the PHJ device is on the order of 10^{12} Jones in the range from 400 to 1000 nm and 2.7×10^{12} Jones at 890 nm. This is among the highest detectivities reported for small-molecule OPDs,[13−18] which makes it favorable for application in panchromatic photodetector. D^* of the PM-HJ 5 device reaches 4.2×10^{12}

DOI: 10.1021/am5074479
ACS Appl. Mater. Interfaces 2015, 7, 2529–2534

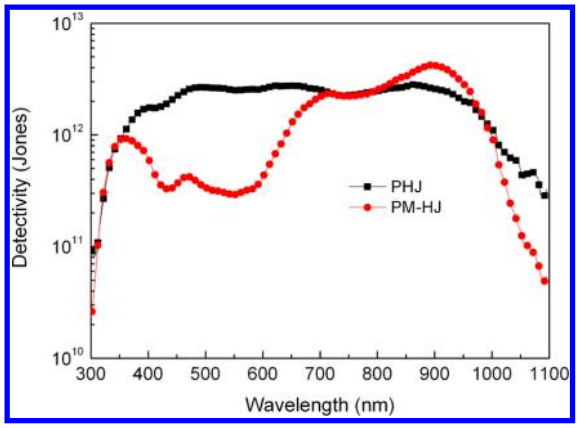

Figure 7. D^* of PHJ device ITO/MoO_3 (2 nm)/CuI (2 nm)/PbPc (60 nm)/C_{70} (60 nm)/Bphen (10 nm)/Al (100 nm) and PM-HJ 5 device ITO/MoO_3 (2 nm)/CuI (2 nm)/PbPc (20 nm)/PbPc:C_{70} (80 nm, 5%:95%)/C_{70} (20 nm)/Bphen (10 nm)/Al (100 nm).

Jones at 890 nm because its EQE is markedly higher compared with that of the PHJ device.

4. CONCLUSION

In summary, high response and D* panchromatic OPDs with PbPc and C_{70} as the D and A, respectively, were demonstrated with PHJ and PM-HJ structures. Both the PHJ and the PM-HJ devices showed broad-band responses from 300 to 1100 nm. An EQE exceeding 10% was obtained for the wavelength region from 400 to 900 nm for the PHJ device. The EQE in the NIR region was enhanced by using the PM-HJ device structure, and a maximum EQE of 30.2% at 890 nm was obtained for the optimized device containing a C_{70} layer doped with 5% PbPc, which is the highest of the reported OPDs at this wavelength. Triclinic PbPc can be formed in the PbPc:C_{70} mixed film when it was deposited onto a pristine PbPc layer, which increased the absorption of the device in the NIR region. Moreover, the PbPc:C_{70} film showed a high hole mobility even with a low PbPc doping concentration of 5%, which facilitated the transport of photogenerated holes outside the mixed layer. These factors, combined with the increased exciton dissociation efficiency in the mixed layer, resulted in the enhanced response in the NIR region of the devices. The PHJ device showed a high D^* in the order of 10^{12} Jones from vis to NIR regions, which is among the highest detectivities reported for organic small-molecule OPDs. D^* in the NIR region was further increased in the PM-HJ device because of the increased response of this structure compared with the PHJ one. Our findings indicate that the performance of OPDs can be manipulated simply by adjusting device structure.

■ ASSOCIATED CONTENT

Ⓢ Supporting Information

Optical electric field distributions in devices, EQE spectra of devices, and absorption spectra and optical parameters of films. This material is available free of charge via the Internet at http://pubs.acs.org.

■ AUTHOR INFORMATION

Corresponding Authors

* E-mail: suzs@ciomp.ac.cn.
*E-mail: zhangguang@ciomp.ac.cn.
*E-mail: chub@ciomp.ac.cn.

Notes

The authors declare no competing financial interest.

■ ACKNOWLEDGMENTS

This work was supported by the National Natural Science Foundation of China (61107082, 61076047, 11004187, 61376062, and 61376022) and the Science and Technology Development Plan of Jilin Province (20140201094JC).

■ REFERENCES

(1) Dong, H.; Zhu, H.; Meng, Q.; Gong, X.; Hu, W. Organic Photoresponse Materials and Devices. *Chem. Soc. Rev.* **2012**, *41*, 1754−1808.
(2) Baeg, K. J.; Binda, M.; Natali, D.; Caironi, M.; Noh, Y. Y. Organic Light Detectors: Photodiodes and Phototransistors. *Adv. Mater.* **2013**, *25*, 4267−4295.
(3) Su, Z.; Li, W.; Chu, B.; Li, T.; Zhu, J.; Zhang, G.; Yan, F.; Li, X.; Chen, Y.; Lee, C. S. High Response Organic Ultraviolet Photodetector Based on Blend of 4,4′,4″-tri-(2methylphenyl phenylamino) triphenylaine and Tris-(8-hydroxyquinolin) Gallium. *Appl. Phys. Lett.* **2008**, *93*, 103309.
(4) Li, L.; Zhang, F.; An, Q.; Wang, Z.; Wang, J.; Tang, A.; Peng, H.; Xu, Z.; Wang, Y. Organic Ultraviolet Photodetector Based on Phosphorescent Material. *Opt. Lett.* **2013**, *38*, 3823−3826.
(5) Scracco, E.; Bouthinon, B.; Verilhac, J. M.; Celle, C.; Chevalier, N.; Mariolle, D.; Dhez, O.; Simonato, J. P. Work Function Tuning for HighPerformance SolutionProcessed Organic Photodetectors with Inverted Structure. *Adv. Mater.* **2013**, *25*, 6534−6538.
(6) Yang, D.; Ma, D. 1,1-Bis[(di-4-tolylamino)phenyl]cyclohexane for Fast Response Organic Photodetectors with High External Efficiency and Low Leakage Current. *J. Mater. Chem. C* **2013**, *1*, 2054−2060.
(7) Nie, R.; Wang, Y.; Deng, X. Alligned Nanofibers as An Interfacial Layer for Achieving High-detectivity and Fast-response Organic Photodetectors. *ACS Appl. Mater. Interfaces* **2014**, *6*, 7032−7037.
(8) Yao, Y.; Liang, Y.; Shrotriya, V.; Xiao, S.; Yu, L.; Yang, Y. Plastic Near-infrared Photodetectors Utilizing Low Band Gap Polymer. *Adv. Mater.* **2007**, *19*, 3979−3983.
(9) Qian, G.; Davey, J. A.; Wright, J. S.; Wang, Z. Y. Family of Diazapentalene Chromophores and Narrow-band-gap Polymers: Synthesis, Halochromism, Halofluorism, and Visible-near Infrared Photodetectivity. *Chem. Mater.* **2012**, *24*, 2364−2372.
(10) Gong, X.; Tong, M.; Xia, Y.; Cai, W.; Moon, J. S.; Cao, Y.; Yu, G.; Shieh, C. L.; Nilsson, B.; Heeger, A. J. High-detectivity Polymer Pthotodetectors with Spectral Response from 300 to 1450 nm. *Science* **2009**, *365*, 1665−1667.
(11) Hu, X.; Dong, Y.; Huang, F.; Gong, X.; Cao, Y. Solution-processed high-detectivity near-infrared polymer photodetectors fabricated by a novel low-bandgap semiconducting polymer. *J. Phys. Chem. C* **2013**, *117*, 6537−6543.
(12) Hendriks, K. H.; Li, W.; Wienk, M. M.; Janssen, R. A. J. Small-Bandgap Semiconducting Polymers with High Near-Infrared Photoresponse. *J. Am. Chem. Soc.* **2014**, *136*, 12130−12136.
(13) Zimmerman, J. D.; Diev, V. V.; Hanson, K.; Lunt, R. R.; Yu, E. K.; Thompson, M. E.; Forrest, S. R. Porphyrin-tape/C_{60} Organic Photodetectors with 6.5% External Quantum Efficiency in the Near Infrared. *Adv. Mater.* **2010**, *22*, 2780−2783.
(14) Zimmerman, J. D.; Yu, E. K.; Diev, V. V.; Hanson, K.; Thompson, M. E.; Forrest, S. R. Use of Additives in Porphyrin-tape C_{60} Near-infrared Photodetectors. *Org. Electron.* **2011**, *12*, 869−873.
(15) Beverina, L.; Ruffo, R.; Salamone, M. M.; Ronchi, E.; Binda, M.; Natali, D.; Sampietro, M. Panchromatic Squaraine Compounds for Broad Band Light Harvesting Electronic Devices. *J. Mater. Chem.* **2012**, *22*, 6704−6710.
(16) Li, L.; Huang, Y.; Peng, J.; Cao, Y.; Peng, X. Highly Responsive Organic Near-infrared Photodetectors Based on a Porphyrin Small Molecule. *J. Mater. Chem. C* **2014**, *2*, 1372−1375.

DOI: 10.1021/am5074479
ACS Appl. Mater. Interfaces 2015, 7, 2529−2534

(17) Qi, J.; Ni, L.; Yang, D.; Zhou, X.; Qiao, W.; Li, M.; Ma, D.; Wang, Z. Panchromatic Small Molecules for UV-Vis-NIR Photodetectors with High Detectivity. *J. Mater. Chem. C* **2014**, *2*, 2431−2438.
(18) Menke, S. M.; Pandey, R.; Holmes, R. J. Tandem Organic Pthotodetectors with Tunable, Broadband Response. *Appl. Phys. Lett.* **2012**, *101*, 223301.
(19) Sakurai, T.; Ohashi, T.; Kitazume, H.; Kubota, M.; Suemasu, T.; Akimoto, K. Structural Control of Organic Solar Cells Based on Nonplanar Metallophthalocyanine/C_{60} Heterojunctions Using Organic Buffer Layers. *Org. Electron.* **2011**, *12*, 966−973.
(20) Zhao, W.; Mudrick, J. P.; Zhang, Y.; Hammond, W. T.; Yang, Y.; Xue, J. Enhancing Photovoltaic Response of Organic Solar Cells Using A Crystalline Molecular Template. *Org. Electron.* **2012**, *13*, 129−135.
(21) Vasseur, K.; Broch, K.; Ayzner, A. L.; Rand, B. P.; Cheyns, D.; Frank, C.; Schreiber, F.; Toney, M. F.; Froyen, L.; Heremans, P. Controlling the Texture and Crystallinity of Evaporated Lead Phthalocyanine Thin Films for Near-Infrared Sensitive Solar Cells. *ACS Appl. Mater. Interfaces* **2013**, *5*, 8505−8515.
(22) Kim, T. M.; Shim, H. S.; Choi, M. S.; Kim, H. J.; Kim, J. J. Multilayer Epitaxial Growth of Lead Phthalocyanine and C_{70} using CuBr as a Templating layer for Enhancing the Efficiency of Organic Photovoltaic Cells. *ACS Appl. Mater. Interfaces* **2014**, *6*, 4286−4291.
(23) Wang, X.; Li, H.; Su, Z.; Fang, F.; Zhang, G.; Wang, J.; Chu, B.; Fang, X.; Wei, Z.; Li, B.; Li, W. Efficient Organic Near-infrared Photodetectors Based on Lead Phthalocyanine/C_{60} heterojunction. *Org. Electron.* **2014**, *15*, 2367−2371.
(24) Wang, X.; Fang, F.; Su, Z.; Fang, X.; Zhang, G.; Wang, J.; Wei, Z.; Li, J.; Wang, X. Aluminum-doped Zinc Oxide as Anode for Organic Near-infrared Photodetectors. *J. Phys. D: Appl. Phys.* **2014**, *47*, 335104.
(25) Xue, J.; Rand, B. P.; Uchida, S.; Forrest, S. R. A Hybrid Planar-Mixed Molecular Heterojunction Photovoltaic Cell. *Adv. Mater.* **2005**, *17*, 66−71.
(26) Pfuetzner, S.; Meiss, J.; Petrich, A.; Riede, M.; Leo, K. Improved Bulk Heterojunction Organic Solar Cells Employing C_{70} Fullerenes. *Appl. Phys. Lett.* **2009**, *94*, 223307.
(27) Pettersson, L. A. A.; Roman, L. S.; Inganäs, O. Modeling Photocurrent Action Spectra of Photovoltaic Devices Based on Organic Thin Films. *J. Appl. Phys.* **1999**, *86*, 487−496.
(28) Zhang, M.; Wang, H.; Tian, H.; Geng, Y.; Tang, C. W. Bulk Heterojunction Photovoltaic Cells with Low Donor Concentration. *Adv. Mater.* **2011**, *23*, 4960−4964.
(29) Chen, G.; Sasabe, H.; Wang, Z.; Wang, X. F.; Hong, Z.; Yang, Y.; Kido, J. Co-Evaporated Bulk Heterojunction Solar Cells with 6.0% Efficiency. *Adv. Mater.* **2012**, *24*, 2768−2773.
(30) Pandey, R.; Zou, Y.; Holmes, R. J. Efficient, Bulk Heterojunction Organic Photovoltaic Cells Based on Boron Subphthalocyanine Chloride-C_{70}. *Appl. Phys. Lett.* **2012**, *101*, 033308.
(31) Xiao, X.; Zimmerman, J. D.; Lassiter, B. E.; Bergemann, K. J.; Forrest, S. R. A Hybrid Planar-mixed Tetraphenyldibenzoperiflanthene/C_{70} Photovoltaic Cell. *Appl. Phys. Lett.* **2013**, *102*, 073302.
(32) Zheng, Y. Q.; Potscavage, W. J., Jr.; Komino, T.; Hirade, M.; Adachi, J.; Adachi, C. Highly Efficient Bulk Heterojunction Photovoltaic Cells Based on C_{70} and Tetraphenyldibenzoperiflanthene. *Appl. Phys. Lett.* **2013**, *102*, 143304.
(33) Jin, F.; Chu, B.; Li, W.; Su, Z.; Zhao, B.; Zhang, T.; Yan, X.; Gao, Y.; Wu, H.; Lee, C. S.; Zhu, J.; Pi, H.; Wang, J. The Influence of Donor Material on Achieving High Photovoltaic Response for Organic Bulk Heterojunction Cells with Small Ratio Donor Component. *Org. Electron.* **2013**, *14*, 1130−1135.
(34) Su, Z.; Wang, L.; Li, Y.; Zhang, G.; Zhao, H.; Yang, H.; Ma, Y.; Chu, B.; Li, W. Surface Plasmon Enhanced Organic Solar Cells with a MoO_3 Buffer Layer. *ACS Appl. Mater. Interfaces* **2013**, *5*, 12847−12853.
(35) Sutty, S.; Williams, G.; Aziz, H. Role of The Donor Material and The Donor-acceptor Mixing Ratio in Increasing The Efficiency of Schottky Junction Organic Solar Cells. *Org. Electron.* **2013**, *14*, 2392−2400.
(36) Vandewal, K.; Widmer, J.; Heumueller, T.; Brabec, C. J.; McGehee, M. D.; Leo, K.; Riede, M.; Salleo, A. Increased Open-Circuit Voltage of Organic Solar Cells by Reduced Donor-Acceptor Interface Area. *Adv. Mater.* **2014**, *26*, 3839−3843.
(37) Zheng, Y. Q.; Potscavage, W. J., Jr.; Zhang, Q. S.; Komino, T.; Taneda, M.; Adachi, C. Comparison of Small Amounts of Polycrystalline Donor Materials in C_{70}-based Bulk Heterojunction Photovoltaics and Optimization of Dinaphthothienothiophene Based Photovoltaic. *Org. Electron.* **2014**, *15*, 878−885.
(38) Hiramoto, M.; Kitada, K.; Iketaki, K.; Kaji, T. Near Infrared Light Driven Organic p-i-n Solar Cells Incorporating Phthalocyanine J-aggregate. *Appl. Phys. Lett.* **2011**, *98*, 023302.
(39) Pandey, R.; Gunawan, A. A.; Mkhoyan, K. A.; Holmes, R. J. Efficient Organic Photovoltaic Cells Based on Nanocrystalline Mixtures of Boron Subphthalocyanine Chloride and C_{60}. *Adv. Funct. Mater.* **2012**, *22*, 617−624.
(40) Lunt, R. R.; Benziger, J. B.; Forrest, S. R. Relationship between Crystalline Order and Exciton Diffusion Length in Molecular Organic Semiconductors. *Adv. Mater.* **2010**, *22*, 1233−1236.
(41) Arnold, M. S.; Zimmerman, J. D.; Renshaw, C. K.; Xu, X.; Lunt, R. R.; Austin, C. M.; Forrest, S. R. Broad Spectral Response Using Carbon Nanotube/Organic Semiconductor/C_{60} Photodetectors. *Nano Lett.* **2009**, *9*, 3354−3358.

DOI: 10.1021/am5074479
ACS Appl. Mater. Interfaces 2015, 7, 2529−2534